Phase stability and initial low-temperature oxidation mechanism of Ti2AlC thin films

Jenny Frodelius, Jun Lu, Jens Jensen, Dennis Paul, Lars Hultman and Per Eklund

Original Publication:

Jenny Frodelius, Jun Lu, Jens Jensen, Dennis Paul, Lars Hultman and Per Eklund, Phase stability and initial low-temperature oxidation mechanism of Ti2AlC thin films, 2013, Journal of the European Ceramic Society, (33), 2, 375-382.
http://dx.doi.org/10.1016/j.jeurceramsoc.2012.09.003

Phase stability and initial low-temperature oxidation mechanism of Ti_2AlC thin films

Jenny Frodelius [1)], Jun Lu[1)], Jens Jensen[1)], Dennis Paul[2)], Lars Hultman[1)], Per Eklund[1)]*

[1)] *Thin Film Physics Division, IFM, Linköping University, 581 83 Linköping, Sweden*
[2)] *Physical Electronics USA, 18725 Lake Drive East Chanhassen MN 55317, USA*

**Corresponding author. Email: perek@ifm.liu.se. Telephone +46 13 288940*

Abstract

Ti_2AlC thin films deposited onto Al_2O_3 by magnetron sputtering were used as model for studying the early stages (<15 min) of relatively-low-temperature (500°C) oxidation of Ti_2AlC. The well-defined microstructure of these films forms a surface of valleys, hillocks and plateaus comprised of basal-plane-oriented grains with a fraction of nonbasal-plane-oriented grains with out-of-plane orientation of (1013) and (1016) as shown by x-ray diffraction and s electron microscopy. During oxidation, Al_2O_3 clusters and areas of C-containing titania (TiO_xC_y) are formed on the surface. A mechanism is proposed in which the locations of the Al_2O_3 clusters are related to the migration of Al atoms diffusing out of Ti_2AlC. The Al_2O_3 is initially formed in valleys or on plateaus where Al atoms have been trapped while TiO_xC_y forms by in-diffusion of oxygen into the Al-deficient Ti_2AlC.. At 500 °C, the migration of Al atoms is faster than the oxidation kinetics; explaining this microstructure-dependent oxidation mechanism.

Keywords: Films; Electron microscopy; Carbides; Interfaces; Corrosion

1. Introduction

Ti_2AlC and Ti_3AlC_2 belong to a group of ternary hexagonal phases called $M_{n+1}AX_n$ phases (n = 1, 2, or 3) that consist of a transition metal (M), an A-group element (A), and C and/or N (X) [1,2,3]. In this system, there is also an intergrown phase, $Ti_5Al_2C_3$, with alternating Ti_2AlC-like and Ti_3AlC_2-like stacking [4,5,6], a type of phase known in several MAX systems [7,8,9,10], but $Ti_5Al_2C_3$ is to date the only one synthesized in bulk with full structure determination [5]. Ti_2AlC and Ti_3AlC_2 are promising materials for applications that demand stability at high temperatures and resistance against oxidation. Many oxidation studies of bulk Ti_2AlC and Ti_3AlC_2 have focused on high temperature (> 1000 °C) oxidation over long periods of time (days) [11,12]. At these elevated temperatures, a protective α-Al_2O_3 layer is formed on the surface [13,14]. The minimum temperature for formation of such a continuous protective layer is at least 700 °C [15]. During growth of the α-Al_2O_3 layer, TiO_2 forms on top of the Al_2O_3 scale as a result of Ti diffusion through the Al_2O_3 layer to the surface where it reacts with oxygen [16,17]. Once the α-Al_2O_3 has grown to sufficient thickness, it will protect against further oxidation of the underlying Ti_2AlC on the condition that the latter is sufficiently phase-pure [18,19,20]. Furthermore, Ti_2AlC has a thermal expansion coefficient similar to Al_2O_3, an important fact that permits the material to be thermally cycled without spalling off the protective oxide [21].

Although the oxidation mechanisms of bulk Ti_2AlC and Ti_3AlC_2 at high temperature and long oxidation times are well understood, the conditions during the initial oxidation stages are unclear. For fractured Ti_3AlC_2 surfaces with oxidation times of 20 s up to 15 min at 1100 °C, Song et al. [22] described how α-Al_2O_3 mainly forms on the basal planes and on

the ledges to the fractured surfaces (also relevant for crack healing [23] and ultrahigh temperature ablation [24]). Oxidation at lower temperatures (500-600 °C) is, however, different from that at high temperatures and tends to result in phase-mixed, porous, oxide layers with non-protective properties [25,26]. The phase purity is also an important factor to obtain good oxidation properties [27].

The purpose of this paper is to improve the understanding of the early stage of oxidation of Ti_2AlC at low temperatures. The experiments are performed at 500 °C to remain well below the 700 °C at which a protective Al_2O_3 layer is formed, but simultaneously high enough to have appreciable oxidation kinetics. Short oxidation times (5 – 15 min) in ambient air are investigated to capture different oxidation stages using scanning electron microscopy and Auger nanoprobe. Magnetron sputtered thin films on single-crystal Al_2O_3(0001) substrates are chosen as they form a well-defined model system for studying microstructural effects on oxidation.

2. Experimental Details

2.1 Synthesis

Ti_2AlC thin films were deposited by magnetron sputtering at a substrate temperature of 770 °C. A TiC seed layer was used to improve the crystal quality of Ti_2AlC grown onto Al_2O_3(0001). The substrates were cleaned in acetone and isopropanol in an ultrasonic bath and heat treated in-situ before deposition. The thin films were deposited from three circular

elemental targets; a 3" Ti target, a 2" Al target and a 3" C target, operated in constant current mode. Deposition of TiC was made at a power density of ~3.0 W/cm^2 for Ti and ~5.6 W/cm^2 for C. The power density for depositing Ti_2AlC was kept at ~2.8 W/cm^2 for Ti, ~1.2 W/cm^2 for Al, and ~3.5 W/cm^2 for C. All targets were facing the substrate from underneath where the Al target was mounted on axis while both Ti and C target was mounted with an off axis angle of 35°. More information about the setup can be found in Ref. 28. The vacuum chamber had a base pressure of ~10^{-6} Pa ($4 \cdot 10^{-8}$ mbar) and the sputtering was performed with Ar gas (99.9999 %) at a pressure of 0.5 Pa (4 mTorr).

2.2 Vacuum Annealing and Oxidation

X-ray diffraction (XRD) measurements (Philips PW 1729) were performed *in situ* during annealing of thin films using a CuKα radiation. Heating of the sample took place in a water cooled vacuum chamber with a base pressure of 10^{-3} Pa. The samples were placed on a Ta filament surrounded by a second Ta filament. Both filaments were resistively heated and connected to Pt/Rh thermocouples to monitor the temperature. The temperature was calibrated using a pure Al_2O_3 plate as reference to record the peak shifts with temperature [29]. One scan was made before annealing at ambient temperature. Then the heater was ramped with ~50 °C/min up to the desired temperature in the range of 300 – 900 °C. A set of 3 scans (15 min each) was started 5 min after reaching the chosen temperature.

Two samples were oxidized in ambient air in a quartz-tube furnace at 500 °C±5 °C. The quartz tube containing a sample was not inserted in the oven until the temperature was

stabilized. The temperature was measured with a thermocouple placed near the sample. When the quartz tube with the sample was inserted in the furnace, the sample reached a temperature of 500 °C after 12.5 min with ambient air present. After additional 5 or 15 min of oxidation in ambient air the quartz tube with the sample was taken out and cooled outside the furnace.

2.3 Characterization

The phase composition of the thin films was characterized by x-ray diffraction (XRD) analysis (Philips PW 1729) with a line-focus CuK_{α} source operating at 40 mA and 40 kV. Pole figure measurements were performed in an x-ray diffractometer (Philips X'Pert MRD) with a point focused CuK_{α} source operating at 40 mA and 45 kV.

All scanning electron microscopy (SEM) images were performed (LEO 1550) with an SE2 secondary electron detector. The working distance was kept at 6 mm and the incoming electron beam at 2 keV. This low acceleration voltage was used to enhance the imaging of details on the surface.

Bright-field transmission electron microscopy (TEM) imaging was performed with a 200 kV field emission gun microscope (Tecnai G2 F20U-Twin). Cross-sectional samples were prepared using focused ion beam (FIB, Carl Zeiss CrossBeam 1540 EsB) with lift-out technique. The sample was cut out with Ga ions using an acceleration voltage of 30 keV, finishing off with 5 keV.

Elemental surface mapping and localized sputter depth profiles were performed with a PHI 700*Xi* Scanning Auger Nanoprobe from Physical Electronics. The Auger spectra were obtained using a 10 keV e-beam with a current of 10 nA and beam size of 22 nm. The sample was tilted 30° with respect to the electron gun. The electron gun is located co-axial to the cylindrical mirror analyzer (CMA) minimizing shadowing effects caused by topography. Sputter profiling was achieved with a 500 eV Ar ion beam hitting the sample at 42° with respect to the surface normal. The sputter rate is roughly 2.5 nm/minute calibrated for SiO_2.

3. Results and Discussion

3.1 As-deposited thin films

Figure 1 shows a typical x-ray diffraction pattern of an as-deposited Ti_2AlC thin film. The $Ti_2AlC(0001)$ planes are parallel with the substrate surface of $Al_2O_3(0001)$ as expected for the epitaxial growth mode [4]. The Ti_2AlC 0006 peak may be overlapped with 1013 (International Centre of Diffraction Data JCPDS 29-0095), since the Ti_2AlC 1013 and 0006 peaks are located close to each other at 2θ values of 39.5° and 39.7°, respectively. The difference of 0.2° is too small to be resolved by XRD. There is, however, a peak at 53.3° (not shown in Figure 1) originating from 1016. The peak is small, as expected from the

structure factor. Pole figure measurements of both 0002 and 1016 show no other orientations than what is observed from the θ/2θ scan. The TiC 111 peak originates from the seed layer and pole figure measurements (not shown, essentially identical to Fig 1e in Ref. 30) show that the TiC is epitaxially grown onto the substrate with two sets of domains with three-fold symmetry.

In general, the growth of thin film MAX phases is dependent on the substrate temperature [1,31,32,33]. Substrate temperatures of ~900 °C promote basal-plane-oriented Ti_2AlC growth [4]. Lower temperatures, on the other hand, may result in nonbasal-oriented growth, even nearly perpendicular basal planes to the substrate surface, as has been observed for Ti_2AlN [33] and Cr_2GeC [34] (cf., also the discussion on growth and epitaxy in Refs. [35,36]). Figure 2 a) shows a SEM image of the top surface of an as-deposited Ti_2AlC thin film. The main part of the surface is flat as a result of (0001) basal-plane-oriented epitaxial Ti_2AlC. In addition, the surface exhibits numerous nonbasal-plane-oriented grains including (1013) and (1016) (cf. Figure 1). At our substrate temperature of 770 °C, it is likely that the basal plane growth does not result in full coverage due to the limited mobility of the ad-atoms. With increasing supersaturation at the reduced temperature, nucleation of nonbasal grain may occur. By virtue of their relatively fast growth, such grains will prevail. Figure 2 b) shows a higher magnification view of a typical flat area, which reveals the presence of basal-plane terraces. These form surface hillocks with hexagonal shapes characteristic of the crystal structure of Ti_2AlC. The way that the terraces of the basal planes have spread indicates that these areas have grown in Frank-van der Merwe (layer-

by-layer) mode or possibly step-flow mode. The height of the terraces is in the direction of the c-axis and each terrace should therefore be a discrete number of unit cells [37]. Nonbasal-plane-oriented grains are evenly distributed and stand out from the basal-plane surface showing terraces from basal planes facing upwards. Most of these grains are elongated and are found in one out of three directions, often forming triangles as seen in Figure 2 b). The long sides of the standing grains are aligned with the sides of the hexagonal hillocks. This indicates a three-fold symmetry relation between the standing grains and the TiC seed layer.

Figure 3 a) shows a cross-sectional TEM image of a nonbasal-plane-oriented Ti_2AlC grain surrounded by basal Ti_2AlC grains. The inset in Figure 3 a) is an electron diffraction pattern characteristic of MAX phases from the nonbasal-plane-oriented Ti_2AlC grain [38]. The nonbasal-plane-oriented grain appears to have overgrown the basal grains and is ~0.2 μm higher from substrate to surface forming a plateau. This observation is not surprising, considering that the fastest growth direction for MAX-phases is along the basal planes [39], which in this case points upwards. The nonbasal-plane-oriented grain does not only grow upwards, but also downwards. The downward growth process consumes the seed layer and substrate by a topotactic reaction and creates a void between the grain and the substrate. Yet, the Ti_2AlC film has no porosity except for the intersecting nonbasal grains (triangular pits in Fig. 2b). Growth of Ti_2AlC into Al_2O_3 requires downwards diffusion of Ti and C. The Al and O then presumably move upwards into the Ti_2AlC grain where the oxygen can occupy C vacancies in the Ti_2AlC crystal [28,40]. The possibility of a solid-state reaction between TiC and Al_2O_3 is well known [4,28,40,41]. Note that O has substantial solubility

on C sites in Ti_2AlC (perhaps as much as 25% [40]), but does not form a complete range of solid solutions like nitrogen does [42]. In contrast, the basal-plane-oriented Ti_2AlC grains have a flat interface to the substrate and seem to have grown exclusively on top of the TiC seed layer. However, Figure 3 b) is a cross sectional TEM image of the interfaces between the substrate, seed layer and Ti_2AlC thin film which shows that the substrate and seed layer have reacted and formed extra layers of Ti_2AlC with basal planes along the interface. This Ti_2AlC may contain oxygen as well [4].

3.2 Decomposition of Ti_2AlC thin films

In order to study what happens to the films during annealing in the absence of oxygen, *in situ* annealing of Ti_2AlC thin films in vacuum was performed in the temperature range from ambient to 900 °C. Table 1 shows the XRD intensity ratio of the Ti_2AlC 0002 and TiC 111 peaks.

A constant value of the intensity ratio of 2.4 is observed up to 600 °C. At 700 °C, the ratio decreased to 1.85 and it continues to decrease with increasing temperature. At 900 °C, neither Ti_2AlC 0002 nor Ti_2AlC 0006/1013 is present, while the TiC 111 peak is stronger than in the diffraction patterns at lower temperatures. These results show that initial decomposition of Ti_2AlC in vacuum occurs at temperatures as low as ~700 °C, which is much lower than what has been reported for bulk material of Ti_2AlC [43] and Ti_3AlC_2 [44]. The same difference has been observed for other MAX phases like Ti_3SiC_2 and Cr_2AlC

[37,45]. For instance, Ti_3SiC_2 thin films decompose at 1100 °C [37,46], which is lower than for bulk material. It is explained by the difference in detection sensitivity or chosen thickness criteria and also points out the role of the chemical environment. A parallel can be drawn to earlier oxidation studies of Ti_2AlC where it has been found that to obtain a good oxidation resistance the material must be exposed to temperatures above 700 °C [15]; to obtain sufficient Al mobility for enough Al to reach the surface and form a protective oxide layer.

3.3 Oxidation of Ti_2AlC thin films

Figure 4 a) shows a SEM overview image of an oxidized Ti_2AlC thin film top surface where the oxidation was performed at 500 °C in ambient air during 5 min. The image shows that the film has the same microstructure as before oxidation (c.f. Figure 2), except for the appearance of small round surface features with a diameter of the order of tens of nanometers. These round features have brighter contrast than the surrounding surface, which is likely caused by charging of a non-conductive material such as oxides. Furthermore, the round shape with no facets is expected for amorphous oxides [47], but γ-alumina cannot be excluded. As seen in Figure 4 a), these oxides are gathered in clusters on the surface. The clusters are mainly found at the bottom of the basal-plane terraces in "valleys" where several terraces meet as shown in Figure 4 b). Oxide clusters are also found on terraces surrounding the nonbasal-plane-oriented grains. The clusters are, however, not found on top of the hexagonal hillocks, as seen in Figure 4 c).

Scanning auger nanoprobe was used to obtain well defined elemental surface mapping and depth profile measurements to identify the oxides and the results are presented in Figure 5). Figure 5 a) shows a SEM image of the chosen area of analysis. Figure 5 b) shows an overview of the Ti (green) and Al (red) distribution on the surface obtained by elemental surface mapping and Figure 5 c) shows depth profile measurements of spot 1, 2, and 3 labeled in Figure 5 a) and b). In general the results in Figure 5 a-c) confirm the presence of Al_2O_3 and C-containing Titania (TiO_xC_y) on the surface. As seen in Figure 5 b) the flat areas are covered by either a mix of the oxides or only TiO_xC_y, while the nonbasal-oriented grains are covered by only Al_2O_3. The three depth profile spots represent these three distinct areas. *Spot 1* is found on the flat surface and the elemental mapping (Figure 5 b) show a top surface containing Ti. The depth profile measurement (Figure 5 c), shows that spot 1 has a relatively thick layer of TiO_xC_y on top of the Ti_2AlC with a thinner area of Al_2O_3 adjacent to the Ti_2AlC interface. The TiO_xC_y has been formed by the remains of Ti_2AlC after the loss of Al. The thick TiO_xC_y oxide has been able to form since a lot of Al has been released instead of forming a protective Al_2O_3 scale on the surface. There are several patches similar to spot 1 on the flat surface and these areas are most likely represented by hillocks as presented in Figure 6. *Spot 2* is also found on the flat surface but is covered by a mix of Al_2O_3 and TiO_xC_y, see Figure 5 b), thus the oxide is not as thick as for spot 1. *Spot 3* represent the nonbasal-oriented grains as seen in Figure 5 a), which has a top layer of Al_2O_3 on top of TiO_xC_y, see Figure 5 c).

We propose that the oxides seen in Figure 4 are dominated by Al_2O_3. To form clusters of Al_2O_3 at these specific areas on the surface, Al diffuses out of the crystal and migrates over

the surface. It is known that the A element diffuses via the basal planes during decomposition of MAX phases [1,2,37,48,49] , since Al has a weaker bond to Ti compared to C. Al is also predicted to have relatively low activation energy for migration in the crystal [50]. The release of Al usually occurs at elevated temperatures, but as demonstrated above, initial decomposition of Ti_2AlC can occur already at 700 °C and possibly at even lower temperatures. A second driving force for Al to exit the crystal could be the presence of oxygen. Therefore, Al can diffuse out from the Ti_2AlC crystal already at 500 °C. However, the migration of Al appears to be faster at 500 °C than the kinetics for oxidation, where the Al migrates on the surface in a liquid-like manner until it is trapped in the valleys, before it reacts with oxygen. In parallel, the Al vacancies formed in the Ti_2AlC crystals enable oxygen in-diffusion, which promotes further oxidation to form TiO_xC_y and maybe also $CO_2(g)$.

Based on the observations above, we infer that the oxidation mechanism of Ti_2AlC in air at 500 °C proceeds as presented in Figure 6:

Step I: Out-diffusion of Al from Ti_2AlC takes place preferentially along the crystal basal planes and the grain boundaries. The Al on the surface will not evaporate since the partial vapor pressure for Al is much lower than the chamber pressure at these temperatures.

Step II: Al moves along the terraces and gathers in the valleys or gets trapped on top of the nonbasal-oriented grains.

Step III: Oxygen from the atmosphere reacts with the Al and forms amorphous Al_2O_3 rounded mounds with size in the tens of nanometer range.

Step IV: When the oxidation process continues, the Ti_2AlC crystal keeps releasing Al, which continues to fill the valleys and oxidizes.

Figure 7 shows a SEM image of a Ti_2AlC thin film surface oxidized in ambient air at 500 °C for 15 min (i.e. *Step IV*). There are continuous oxide layers covering areas of a width of micrometers in contrast to the small round features as seen for the thin film oxidized for 5 min (c.f. Figure 4). The oxide covers valleys of the original terrace surface and surrounds the nonbasal-plane-oriented grains. This shows that, with time, the oxide formed in the valleys becomes both thicker and spreads out over the Ti_2AlC basal plane surface.

To place these results in relation with known oxidation mechanisms for Ti_2AlC and Ti_3AlC_2 we compare with earlier studies on bulk material. We have observed that during oxidation of Ti_2AlC at lower temperature of 500 °C, clusters of Al_2O_3 are first formed, followed by the formation of TiO_xC_y. However, oxidation studies of bulk Ti_2AlC and Ti_3AlC_2 at 500 °C for 20 min or longer show how a TiO_2 scale (anatase and rutile) form, and that if any Al_2O_3 exists it is expected to be amorphous [25,26]. This means that with time the TiO_2 will be dominant and form a scale on the cost of the formation of Al_2O_3.

Oxidation of Ti_2AlC and Ti_3AlC_2 $\geq$1000 °C has a different outcome. Initial oxidation of Ti_3AlC_2 at 1100 °C results in string-like oxides, assumed to grow along the Al atom planes

of fractured surfaces [22]. One explanation why lower temperatures results in oxide clusters and higher temperatures in string-like oxides is that lower temperature decreases the kinetics of the oxidation reaction and therefore the Al have time to migrate over the surface before reacting with oxygen, while higher temperature leads to an instant formation of oxides as the Al reaches the surface.

Longer oxidation time at temperatures ≥1000 °C results in a dense protective crystalline α-Al_2O_3 scale on top of the Ti_2AlC surface [19]. TiO_2 is instead formed as an outer layer on top of the Al_2O_3 scale as Ti diffuse out through the underlying Al_2O_3 to react with oxygen [19]. Our annealing results explain the difference between the oxide scales of low and high oxidation temperature. A temperature above 700 °C is beneficial for the material to release sufficient amounts of Al fast enough so that a covering scale of Al_2O_3 can form. Below 700 °C the competition between the two oxides is finally won by TiO_2.

4. Conclusions

Ti_2AlC thin films have been used as a model for studying the early stages of oxidation at a relatively low temperature of 500 °C. The thin films have a well defined microstructure of crystalline grains which forms a surface of valleys, hillocks and plateaus. Thus, they constitute an ideal model system for investigating microstructure-dependent oxidation.

During oxidation clusters of Al_2O_3, and C-containing titania (TiO_xC_y) are formed on the surface. It is found that the positions of the Al_2O_3 clusters are related to the migration of the

Al atoms that diffuses out from the Ti_2AlC crystals. The Al_2O_3 is initially formed in the valleys or on the plateaus where the Al-atoms have been trapped while the TiO_xC_y forms by in-diffusion of oxygen into the Al vacancies of the Ti_2AlC crystal. At 500 °C the migration of Al atoms is faster than the formation of Al_2O_3 (low kinetics) and therefore it is possible for TiO_xC_y to form as well. A combination of Al_2O_3 and TiO_xC_y is not beneficial for obtaining a resistance against further oxidation of the material. It is found that the release of Al from Ti_2AlC is most effective at temperatures ≥ 700 °C. A higher rate of out-diffusion of Al to the surface makes it apt to form a covering protective Al_2O_3 scale, and therefore Ti_2AlC requires an oxidation temperature ≥ 700 °C to obtain a good oxidation resistance.

Acknowledgments

N. Ghafoor and P.O.Å Persson at Thin Film Physics (Linköping University) are acknowledged for assistance with TEM. The Swedish National Graduate School in Materials Science is acknowledged for financial support.

References

[1] Eklund P, Beckers M, Jansson U, Högberg H, Hultman L. The $M_{n+1}AX_n$ phases: materials science and thin film processing. *Thin Solid Films* 2010;**518:**1851-78.

[2] Wang JY, Zhou YC. Recent progress in theoretical prediction, preparation, and characterization of layered ternary transition-metal carbides. *Annu Rev Mater Res* 2009;**39**:415-43.

[3] Barsoum MW. The $M_{N+1}AX_N$ Phases: A New Class of Solids; Thermodynamically Stable Nanolaminates. *Prog Solid State Chem* 2000;**28**;201-81.

[4] Wilhelmsson O, Palmquist J-P, Lewin E, Emmerlich J, Eklund P, Persson POÅ, Högberg H, Li S, Ahuja R, Eriksson O, Hultman L, Jansson U. Deposition of ternary thin films within the Ti-Al-C System by dc Magnetron Sputtering. *J Cryst Growth* 2006;**291**:290-300.

[5] Lane NJ, Naguib M, Lu J, Hultman L, Barsoum MW. Structure of a new bulk $Ti_5Al_2C_3$ MAX phase produced by the topotactic transformation of Ti_2AlC. *J Eur Ceram Soc* 2012;**32**: 3485–91.

[6] Lane NJ, Naguib M, Lu J, Eklund P, Hultman L, Barsoum MW. Comment on "$Ti_5Al_2C_3$: A New Ternary Carbide Belonging to MAX Phases in the Ti–Al–C System". *J Am Ceram Soc* 2012, DOI: 10.1111/j.1551-2916.2012.05299.x (2012).

[7] Palmquist JP, Li S, Persson POÅ, Emmerlich J, Wilhelmsson O, Högberg H, Katsnelson MI, Johansson B, Ahuja R, Eriksson O, Hultman L, Jansson U. $M_{n+1}AX_n$ phases in the Ti-Si-C system studied by thin-film synthesis and ab initio calculations. *Phys Rev B* 2004;**70:**165401.

[8] Högberg H, Eklund P, Emmerlich J, Birch J, Hultman L. Epitaxial Ti_2GeC, Ti_3GeC_2, and Ti_4GeC_3 MAX-phase thin films grown by magnetron sputtering. *J Mater Res* 2005;**20**:779-82.

[9] Högberg H, Hultman L, Emmerlich J, Joelsson T, Eklund P, Molina-Aldareguia JM, Palmquist JP, Wilhelmsson O, Jansson U. Growth and characterization of MAX-phase thin films. *Surf Coat Technol* 2005;**193**:6-10.

[10] Scabarozi TH, Hettinger JD, Lofland SE, Lu J, Hultman L, Jensen J, Eklund P. Epitaxial growth and electrical-transport properties of $Ti_7Si_2C_5$ thin films synthesized by reactive sputter-deposition.

Scripta Mater 2011;**65**:811-14.

[11] Wang XH, Zhou YC. Layered Machinable and Electrically Conductive Ti_2AlC and Ti_3AlC_2 Ceramics: a Review. *J Mater Sci Technol* 2010;**26**:385-416.

[12] Wang XH, Li FZ, Chen JX, Zhou YC. Insights into high temperature oxidation of Al_2O_3-forming Ti_3AlC_2. *Corr Sci* 2012;**58**:95-103.

[13] Wang XH, Zhou YC. Oxidation behavior of Ti_3AlC_2 at 1000–1400 °C in air. *Corros Sci* 2003;**45**:891-907.

[14] Yang HJ, Pei YT, Song GM, De Hosson JThM. Comments on "microstructural evolution during high-temperature oxidation of Ti_2AlC ceramics". *Scripta Mater* 2011;**65**:930-32.

[15] Sonestedt M, Frodelius J, Sundberg M, Hultman L, Stiller K. Oxidation of Ti_2AlC bulk and spray deposited coatings. *Corros Sci* 2010;**52:**3955-3961.

[16] Yang HJ, Pei YT, Rao JC, de Hosson JThM, Li SB, Song GM. High temperature healing of Ti_2AlC: On the origin of inhomogeneous oxide scale. *Scripta Mater* 2011;**65**:135-38.

[17] Rao JC, Pei YT, Yang HJ, Song GM, Li SB, de Hosson JThM. TEM study of the initial oxide scales of Ti_2AlC. *Acta Mater* 2011;**59:**5216-5223.

[18] Lee DB, Park SW. High-temperature oxidation of Ti_3AlC_2 between 1173 and 1473 K in air. *Mater Sci Eng A* 2006;**434**:147-154.

[19] Wang XH, Zhou YC. High-Temperature Oxidation Behavior of Ti_2AlC in Air. *Oxid. Met.* 2003;**59**:303-320.

[20] Byeon J, Liu J, Hopkins M, Fischer W, Garimella N, Park KB, Brady MP, Radovic M, El-Raghy T, Sohn YH. Microstructure and Residual Stress of Alumina Scale Formed on Ti_2AlC at High Temperature in Air. *Oxid Met* 2007;**68**:97-111.

[21] Sundberg M, Malmqvist G, Magnusson A, El-Raghy T. Alumina forming high temperature silicides and carbides. *Ceram Int* 2004;**30:**1899-1904.

[22] Song GM, Pei YT, Sloof WG, Li SB, de Hosson JThM, van der Zwaag S. Early stages of oxidation of Ti_3AlC_2 ceramics. *Mater Chem Phys* 2008;**112**:762-8.

[23] Li SB, Song GM, Kwakernaak K, van der Zwaag S, Sloof WG. Multiple crack healing of a Ti_2AlC ceramic. *J Eur Ceram Soc* 2012;**32**:1813-20.

[24] Song GM, Li SB, Zhao CX, Sloof WG, van der Zwaag S, Pei YT, de Hosson JThM. Ultra-high temperature ablation behavior of Ti2AlC ceramics under an oxyacetylene flame. *J Eur Ceram Soc* 2011;**31**:855-62.

[25] Wang XH, Zhou YC. Intermediate-temperature Oxidation Behaviour of Ti2AlC in Air. *J Mater Res* 2002;**17:**2974-81.

[26] Wang XH, Zhou YC. Improvement of intermediate-temperature oxidation resistance of Ti3AlC2 by pre-oxidation. *Mat Res Innovat* 2003;**7:**381-90.

[27] Wang QM, Garkas W, Flores Renteria A, Leyens C, Lee HW, Kim KH. Oxidation behaviour of Ti–Al–C films composed mainly of a Ti2AlC phase. *Corros Sci* 2011;**53:**2948-55.

[28] Frodelius J, Eklund P, Beckers M, Persson POÅ, Högberg H, Hultman L. Sputter-deposition from a Ti_2AlC target: Process characterization and conditions for growth of Ti_2AlC. *Thin Solid Films* 2010;**518**:1621-26.

[29] Reeber RR, Wang K. Lattice Parameters and Thermal Expansion of Important Semiconductors and Their Substrates. *Mater. Res. Soc. Symp.,* 2000;**622**:T6.35.1-6.

[30] Eklund P, Högberg H, Hultman L. Epitaxial TiC/SiC multilayers. *Phys Stat Sol RRL* 2007;**1**:113-5.

[31] Walter C, Sigumonrong D, El-Raghy T, Schneider JM. Towards large area deposition of Cr_2AlC on steel. *Thin Solid Films* 2006;**515**:389-93.

[32] Li JJ, Hu LF, Li FZ, Li MS, Zhou YC. Variation of microstructure and composition of the Cr_2AlC coating prepared by sputtering at 370 and 500 °C. *Surf Coat Technol* 2010;**204**:3838-45.

[33] Beckers M, Höglund C, Baehtz C, Martins RMS, Persson POÅ, Hultman L, Möller W. The influence of substrate temperature and Al mobility on the microstructural evolution of magnetron sputtered ternary Ti–Al–N thin films.*J Appl Phys* 2009;**106**:064915.

[34] Eklund P, Bugnet M, Mauchamp V, Dubois S, Tromas C, Jensen J, Piraux L, Gence L, Jaouen M, Cabioc'h T. Epitaxial growth and electrical transport properties of Cr_2GeC thin films.

Phys Rev B 2011;**84**:075424.

[35] Tucker MD, Persson POÅ, Guenette MC, Rosén J, Bilek MMM, McKenzie D. Substrate orientation effects on the nucleation and growth of the $M_{n+1}AX_n$ phase Ti_2AlC. *J Appl Phys* 2011;**109**:014903.

[36] Eklund P, Murugaiah A, Emmerlich J, Csigany Z, Frodelius J, Barsoum MW, Högberg H, Hultman L. Homoepitaxial growth of Ti-Si-C MAX-phase thin films on bulk Ti_3SiC_2 substrates *J Cryst Growth* 2007;**304**:264-9.

[37] Emmerlich J, Music D, Eklund P, Wilhelmsson O, Jansson U, Schneider JM, Högberg H, Hultman L. Thermal stability of Ti_3SiC_2 thin films. *Acta Mater* 2007;**55:**1479-88.

[38] Lin ZJ, Zhuo MJ, Zhou YC, Li MS, Wang JY. Microstructural characterization of layered ternary Ti_2AlC. *Acta Mater* 2006;**54:**1009-15.

[39] Zhou YC, Dong HY, Yu BH. Development of titanium tin carbide (Ti2SnC) plate based on the electronic structure investigation. *Mater Res Innovat* 2000;**4:**36-41.

[40] Persson POÅ, Rosén J, McKenzie DR, Bilek MMM. Formation of the MAX-phase oxycarbide $Ti_2AlC_{1-x}O_x$ studied via electron energy-loss spectroscopy and first-principles calculations. *Phys Rev B* 2009;**80:**092102.

[41] Persson POA, Rosen J, McKenzie DR, Bilek MMM, Hoglund C. A solid phase reaction between TiC_x thin films and Al_2O_3 substrates. *J Appl Phys* 2008;**103**:066102.

[42] Cabioc'h T, Eklund P, Mauchamp V, Jaouen M. Structural investigation of substoichiometry and solid solution effects in $Ti_2Al(C_x,N_{1-x})_y$ compounds. *J Eur Ceram Soc* 2012;**32:**1803-11.

[43] Pang WK, Low IM. Diffraction Study of Thermal Dissociation in the Ternary Ti-Al-C System. *J Aust Ceram Soc* 2009;**45:**30-33.

[44] Wang XH, Zhou YC. Stability and selective oxidation of aluminum in nanolaminate Ti_3AlC_2 upon heating in argon. *Chem Mater* 2003;**15**:3716-20.

[45] Wang QM, Flores Renteria A, Schroeter O, Mykhaylonka R, Leyens C, Garkas W, to Baben M. Fabrication and oxidation behavior of Cr2AlC coating on Ti6242 alloy.

Surf Coat Technol 2010;**204:**2343-52.

[46] Eklund P, Virojanadara C, Emmerlich J, Johansson LI, Högberg H, Hultman L.

Photoemission studies of Ti_3SiC_2 and nc-TiC/a-SiC nanocomposite thin films.

Phys Rev B 2006;**74**:045417.

[47].Jeurgens LPH, Sloof WG, Tichelaar FD, Mittemeijer EJ. Growth kinetics and mechanisms of aluminum-oxide films formed by thermal oxidation of aluminum. *J Appl Phys* 2002;**92**:1649-56.

[48] Emmerlich J, Eklund P, Rittrich D, Högberg H, Hultman L.

Electrical resistivity of $Ti_{n+1}AC_n$ (A:Si,Ge,Sn) thin films. *J Mater Res* 2007;**22**:2279-87.

[49] Frodelius J, Johansson E, Cordoba Gallego JM, Odén M, Eklund P, Hultman L.

Annealing of thermally sprayed Ti_2AlC coatings. *Int J Appl Ceram Technol* 2011;**8**:74-84.

[50] Music D*,* Riley DP, Schneider JM. Energetics of point defects in TiC. *J Eur Ceram Soc* 2009;**29:**773-7.

Table

Table 1. Ratio between x-ray diffraction peaks acquired during in-situ measurements of a Ti_2AlC film on a TiC seed layer annealed in vacuum.

Temperature (°C)	*$Ti_2AlC(0002) / TiC(111)$*
Ambient	*2.42*
300	*2.43*
500	*2.40*
600	*2.42*
650	*2.33*
700	*1.85*
750	*1.22*
800	*0.70*
850	*0.33*

Figure captions

Figure 1. X-ray diffractogram of a Ti_2AlC thin film with a TiC seed layer deposited onto a single crystalline Al_2O_3(0001) substrate.

Figure 2. SEM images of the top surface of a Ti_2AlC thin film where a) shows an overview, and b) hexagonal shaped hillocks and triangles.

Figure 3 a). Bright-field TEM cross-sectional image of a Ti_2AlC grain showing how the basal planes are standing up from the Al_2O_3 substrate surface and spreads out over the surrounding epitaxially grown Ti_2AlC grains. The inset is a diffraction pattern from the standing grain. b). Interface between substrate (Al_2O_3), seed layer (TiC) and Ti_2AlC showing reaction between substrate and seed layer resulting in the formation of an interfacial layer of Ti_2AlC.

Figure 4. SEM image of an Ti_2AlC thin film oxidized in ambient air at 500 °C for 5 min showing a) overview, b) oxide clusters, and c) hexagonal shaped hillock free of the oxide clusters.

Figure 5. a) SEM-image overview of an area on the Ti_2AlC thin film oxidized in ambient air at 500 °C for 5 min measured with scanning auger nanoprobe b) distribution of Ti (green) and Al (red) and depth profiles from c) spot 1, d) spot 2, and e) spot 3 marked in the SEM image..

Figure 6. Illustration of the initial oxidation mechanism of Ti_2AlC thin films in ambient air at 500 °C. Al leaves the Ti_2AlC crystal via the basal planes (Step I), migrates down the terraces where it gathers in the valleys (Step II), and reacts with oxygen to form amorphous Al_2O_3 (Step III). With time, the oxide grows thicker and spreads out over the terraces (Step IV).

Figure 7. SEM image of a Ti_2AlC thin film surface oxidized in ambient air at 500 ° for 15min.

Figure 1
Click here to download high resolution image

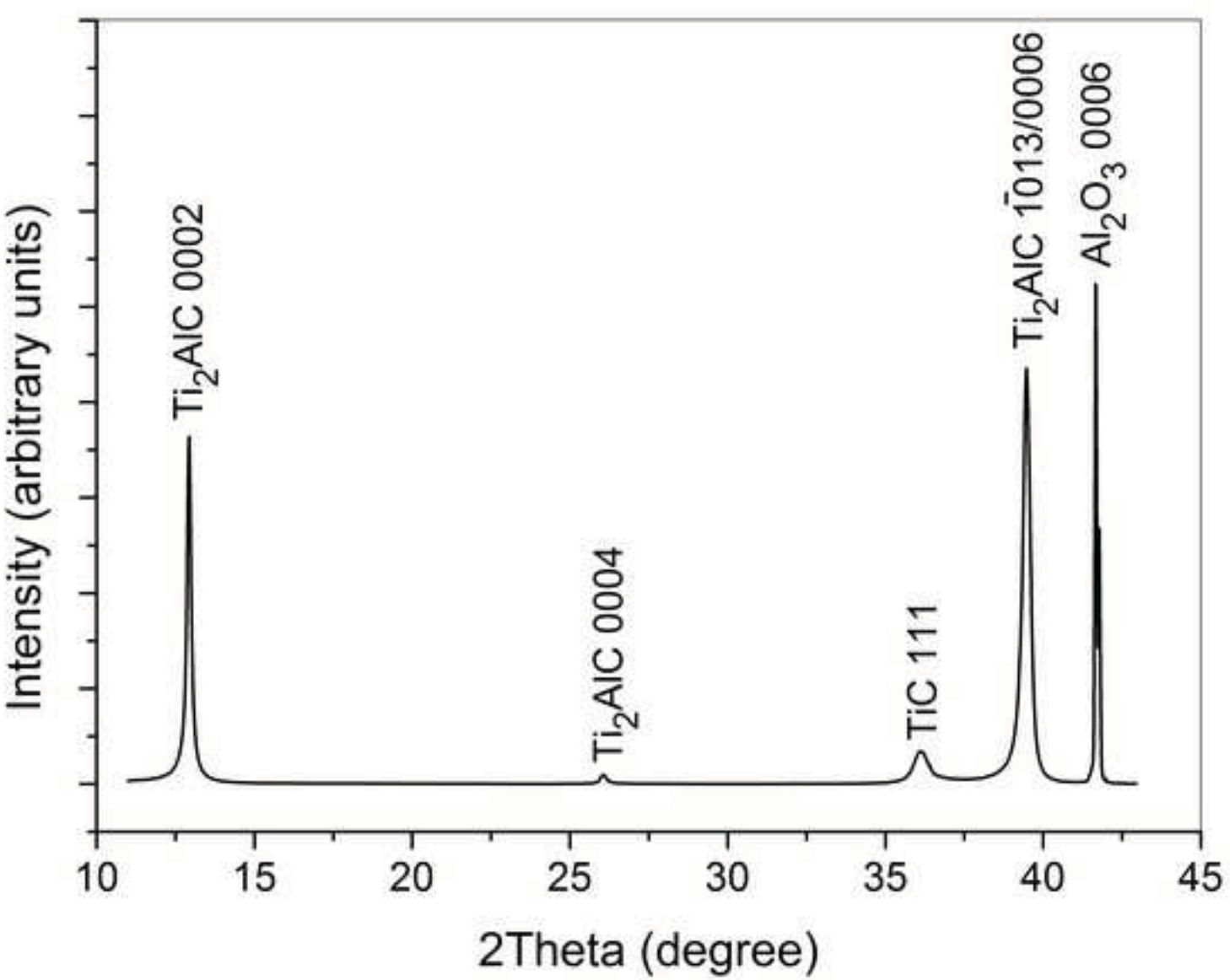

Figure 2
Click here to download high resolution image

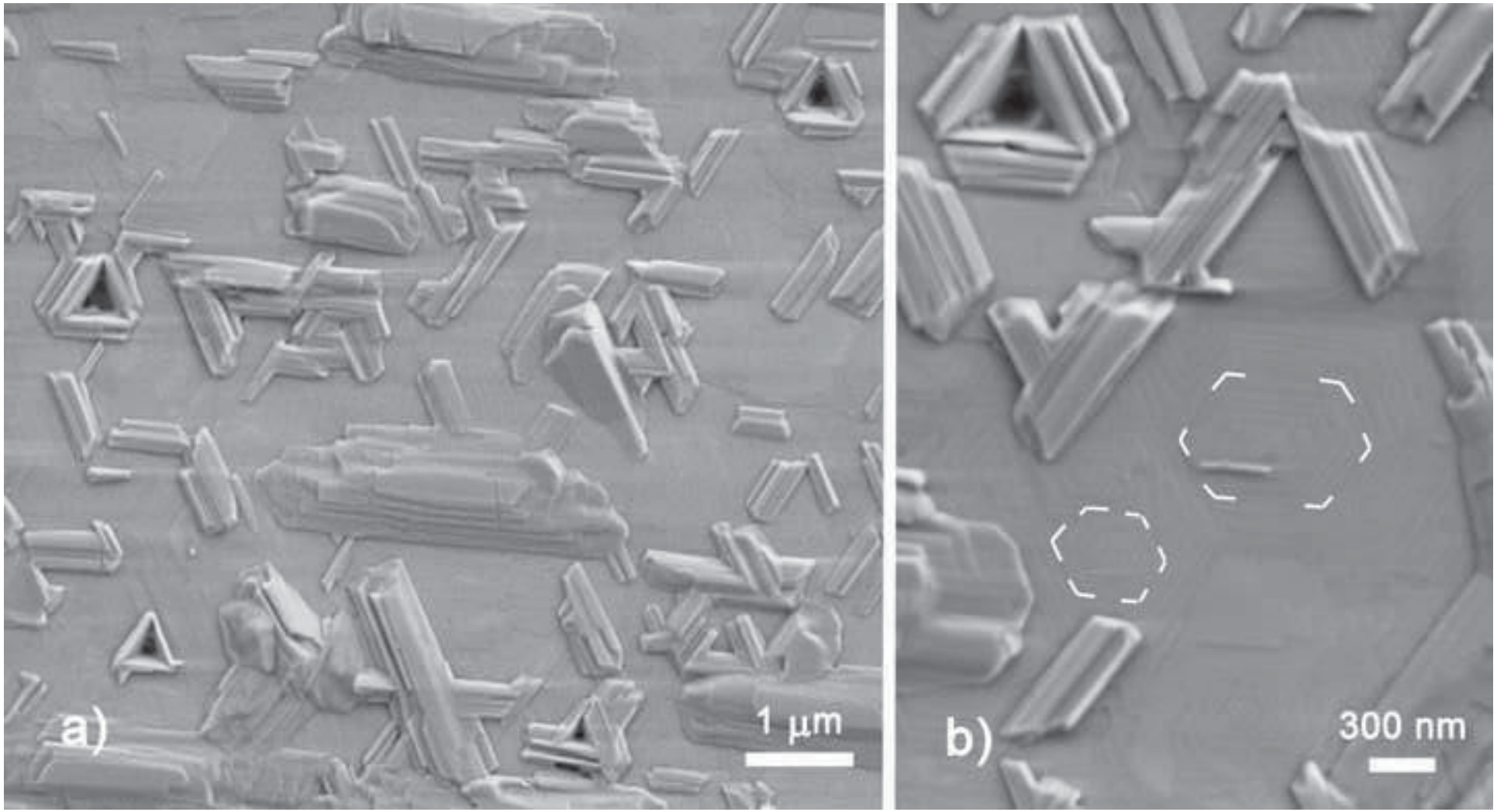

Figure 3
Click here to download high resolution image

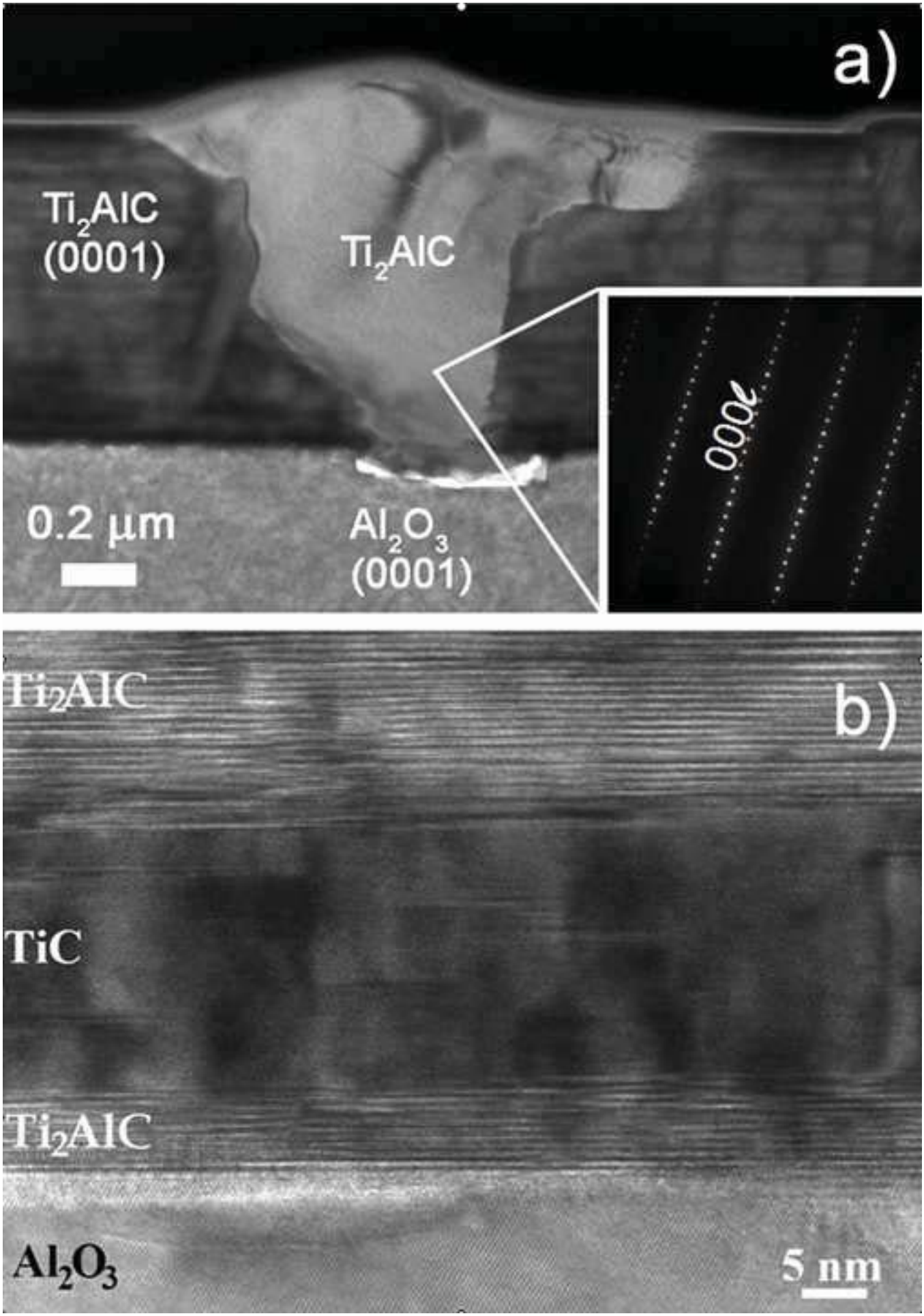

Figure 4
Click here to download high resolution image

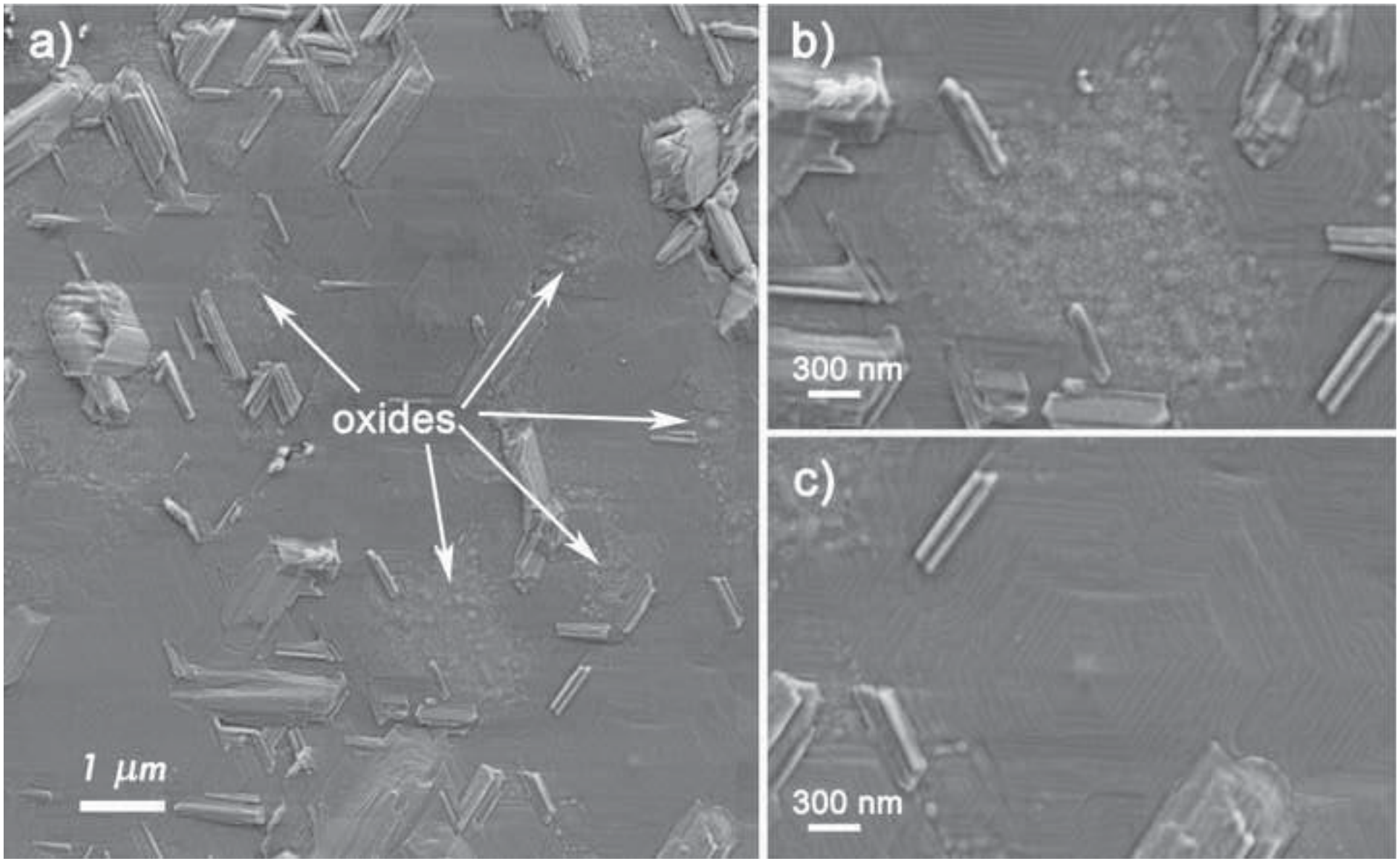

Figure 5ab
Click here to download high resolution image

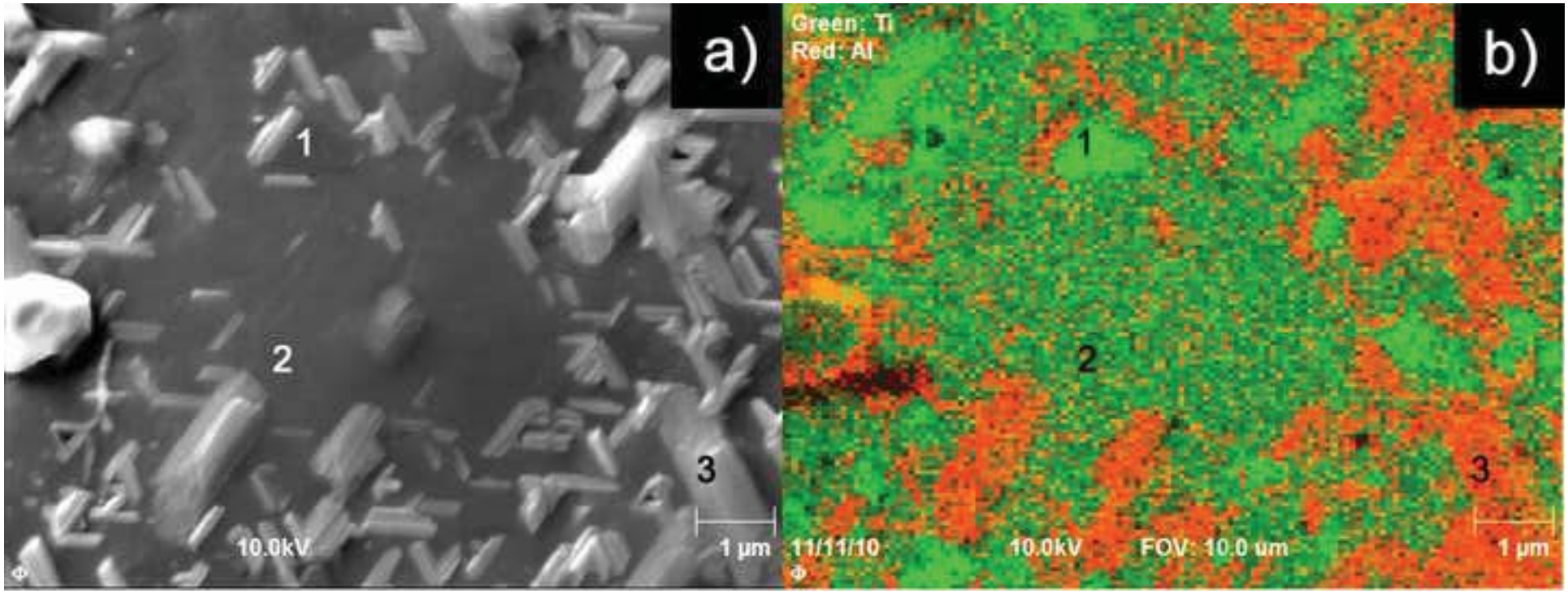

Figure 5c

Click here to download high resolution image

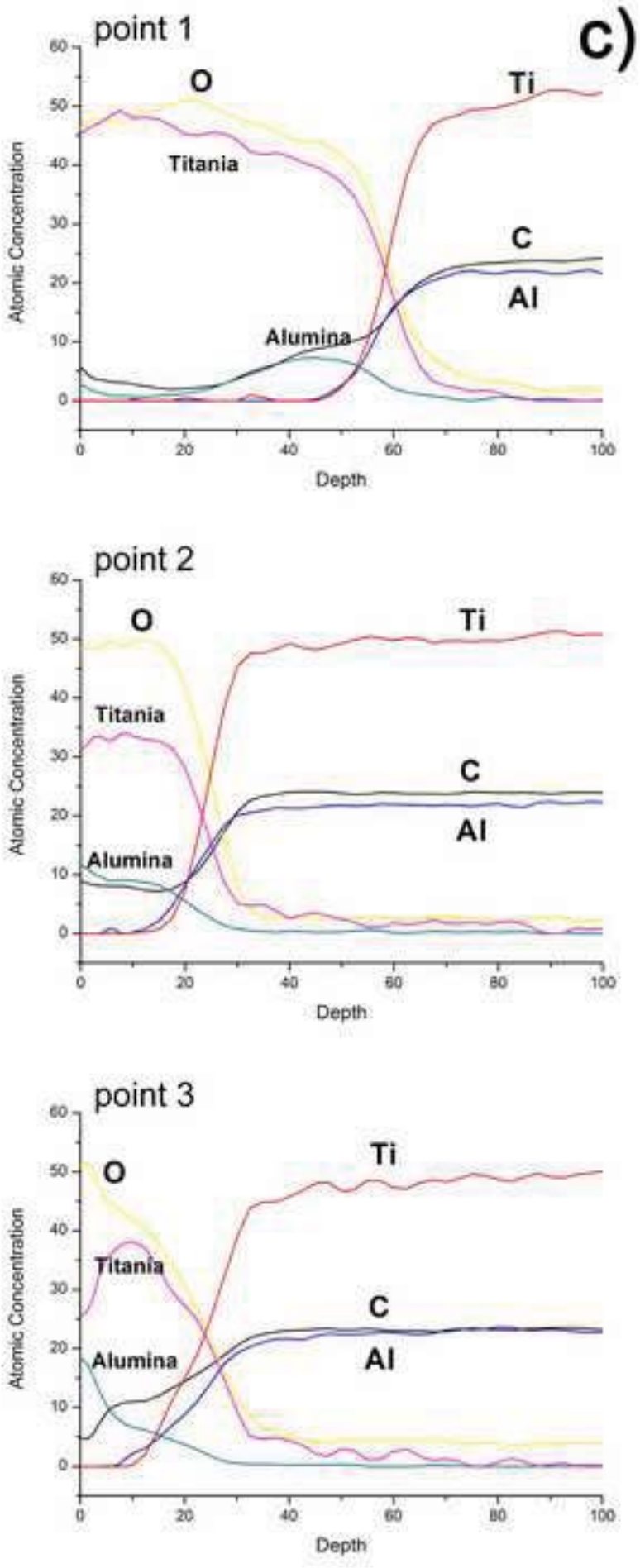

Figure 6
Click here to download high resolution image

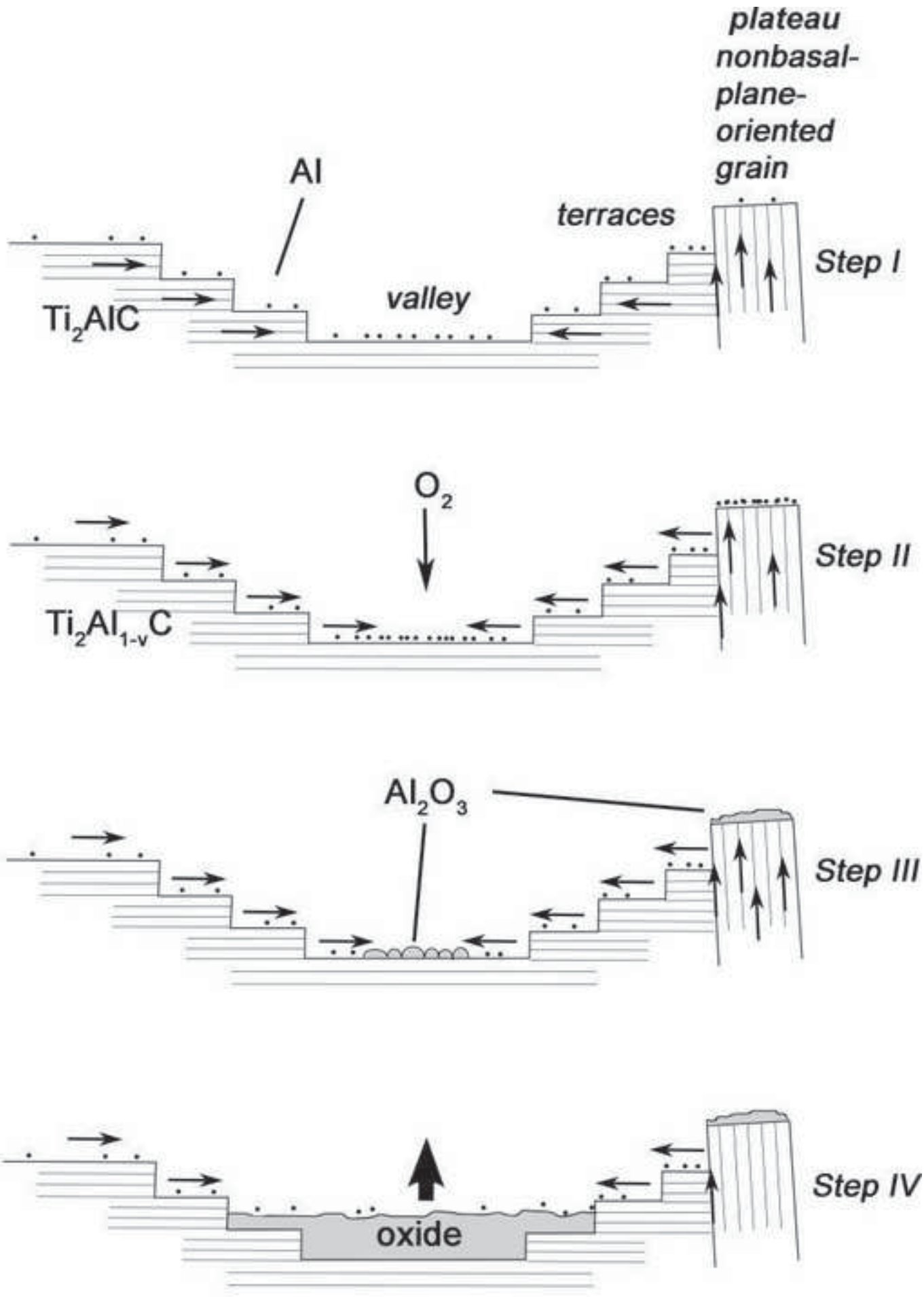

Figure 7

Click here to download high resolution image